J Nanopart Res (2024) 26:44
https://doi.org/10.1007/s11051-024-05945-0

RESEARCH

A way to prepare magnetically separable palladium nanocatalysts active in Heck reaction—SI-RAFT/MADIX polymerization for modification of magnetic nanoparticles

Iwona Misztalewska-Turkowicz · Sławomir Wojtulewski · Agnieszka Z. Wilczewska

Received: 28 November 2023 / Accepted: 5 February 2024 / Published online: 26 February 2024

Abstract In terms of sustainable and "green" chemistry, recovery and reuse of the catalysts plays an important role. Easily recoverable heterogeneous catalysts are now a highly studied topic. Considering it, we have investigated magnetic iron oxide nanoparticles covered by polymeric shells with random structures as solid support for palladium catalysts. Polymerizable imidazolium derivative was synthesized to form imidazolium salt (N-heterocyclic carbene precursor) with an unsaturated vinyl bond. Subsequently, two different palladium salts were used to form palladium complexes on the solid surface. Two catalyst forms were produced depending on the palladium salt used: catalysts with N-heterocyclic carbene-palladium complexes and palladium nanoparticles (formed in situ, without the application of any reductive agent). Synthesized complexes were tested on their activity toward the Heck cross-coupling reaction, and the recyclability of chosen ones was also studied. The obtained polymeric-inorganic hybrids were characterized using FT-IR spectroscopy, SEM/EDX and TEM microscopy, XRD diffraction, and TGA thermal analyses.

Keywords Nanostructured catalysts · Magnetic nanoparticles · Heterogeneous catalysis · Heck cross-coupling reaction · SI-RAFT/MADIX polymerization

Supplementary Information The online version contains supplementary material available at https://doi.org/10.1007/s11051-024-05945-0.

I. Misztalewska-Turkowicz (✉) · A. Z. Wilczewska
Department of Organic Chemistry, Faculty of Chemistry, University of Bialystok, K. Ciołkowskiego 1K, 15-245 Białystok, Poland
e-mail: i.misztalewska@uwb.edu.pl

S. Wojtulewski
Department of Physical Chemistry, Faculty of Chemistry, University of Bialystok, K. Ciołkowskiego 1K, 15-245 Białystok, Poland

Introduction

A sustainable approach for industrial processes comes from researchers searching for better, "greener" solutions for known issues. One of those issues is a catalytic process. Strict expectations for modern catalysts put the ability for easy recovery and efficient reuse of catalysts as their highly desirable feature. Generally, catalysts are divided into two groups—homogeneous and heterogeneous catalysts. Homogeneous catalysts are well-defined and soluble in the reaction medium species. These features cause high accessibility to the starting materials, which often force high catalytic activity and selectivity, even under mild conditions [1]. Beyond their excellent characteristics, homogeneous catalysts have some drawbacks in terms of sustainability. They are difficult to separate and recover from the reaction mixture, which results in environmental pollution, corrosion, and deposition on the reactor walls, which causes high economic

costs and limits their applications in industry [2]. Though heterogeneous catalysts are usually less efficient than homogeneous ones, their easy recovery is the predominant benefit. The gap between heterogeneous and homogeneous catalytic processes can be filled by applying nanocatalysis, e.g., nanoparticles as solid phase carriers for the catalyst [3]. Nanoparticles are unstable since they have a large surface-to-volume ratio (a large part of their atoms are presented on their surface). They must be stabilized by capping agents such as polymers [4], surfactants [5], dendrimers [6], or ionic liquids [7–9]. Among the variety of nanoparticles (metallic, polymeric, etc.), magnetic nanoparticles (especially iron oxide nanoparticles) are one of the most frequently used for immobilizing catalysts. They are non-toxic, readily available, and easy to modify by applying coating agents [10–12]. Usually, magnetic nanoparticles (NPs) are first coated with silica to form magnetic core–shell structures. The coating provides (besides the stabilization of nanoparticles) the possibility of the introduction of functional groups, which allow the attachment of various catalytic species on the NPs surface, including ligands that possess good complexing activity (for example, N-heterocyclic carbenes—NHCs [13, 14]) [3]. Since the past 30 years (since the first isolation of stable carbene by Arduengo et al. [15]), N-heterocyclic carbene ligands have been broadly used in transition metal complexes and as organocatalysts. NHCs are versatile ligands not only for forming organometallic complexes [16] but also for stabilizing metal nanoparticles for nanocatalysis [17–19]. Herein, we choose an NHC polymerizable precursor to form a polymer coating with complexing activity.

The application of transition metal nanocatalysts in organic reactions, especially those providing new C–C bonds (e.g., the Suzuki, Heck, and Sonogashira cross-coupling reactions), has riveted utmost attention because of their high surface area, a large number of catalytic active centers, and chemical stability [20–22]. The most used complexes are homogenous palladium catalysts. Their application benefits in many aspects but also has critical drawbacks, e.g., purification of product from palladium residue and virtually any reapplication possibility due to the formation of inactive Pd black. For those reasons, palladium complexes on a solid phase (e.g., magnetic nanoparticles) are being studied increasingly as efficient and recyclable catalysts [23–26]. One of the immobilization methods of palladium into nanoparticles is radical polymerization techniques [27–30], among which Surface Initiated Reversible Addition Fragmentation Chain Transfer (SI-RAFT) polymerization plays a vital role [31]. Coating nanoparticles by polymeric chains with defined structures causes extended durability of the system in various conditions and facilitates the reusability of the metallic catalysts [32]. However, in some cases, the polymeric coating may cause a reduction of catalytic efficiency because of the burying of catalytic sites in the polymer backbone, thus limiting the access of reactants [33]. This limitation occurs when a polymerizable catalyst is used as a monomer in a polymerization reaction. It is rarely possible when a catalyst is prepared in the post-modification step of a polymeric shell (as presented in this work)—modification occurs only at accessible places. In the recent literature, only several papers describing the application of polymer-modified magnetic nanoparticles as carriers for palladium catalysts used in C–C coupling reactions can be found. Ghasemi et al. used magnetite nanoparticles modified by thermoresponsive copolymer (PNIPAM) decorated by palladium nanoparticles for the Heck reaction. In the results described, high conversions were obtained even with a low amount of the catalyst. The polymeric shell was prepared by free radical polymerization; thus, the reaction occurred both in solvent and on the surface of the nanoparticles. Consequently, the authors needed to use a high excess of monomers [34]. Yang et al. applied magnetite nanoparticles modified by formaldehyde resin and thermoresponsive part to produce the catalyst active in Suzuki reaction. This system showed the influence of the catalyst activity in dependence on the temperature (better activity below the LCST of PNIPAM) [35]. Furthermore, a polycondensation reaction was used to modify magnetic nanoparticles. The combination of citric acid and PEG led to the production of magnetic nanoparticles covered by hyperbranched polymer capable of stabilization of Pd nanoparticles [36]. Subsequently, polydopamine was used as MNP modifier and Pd complexing agent. The large aggregates contained Pd nanoparticles possessed good activity in the Buchwald-Hartwig reaction [37]. Recently, we applied SI-RAFT/MADIX polymerization for the preparation of magnetically separable Pickering interfacial catalyst active in water in the Suzuki reaction [38].

The polymeric materials used in organometallic catalysis prepared by controlled radical polymerization have many valuable functions, e.g., they are stable, introduce to the system various functional groups (their structure is limited only by the limitations resulting from organic synthesis) [39], and differ structures (e.g., homopolymers or copolymers), which influences their physicochemical properties [40]. These features significantly improve the final properties of the synthesized catalysts, enabling, for example, attachment of many active sites, tuning of chain solubility, or bringing a response to external stimuli (e.g., thermosensitive polymers [41]). Using magnetic nanoparticles significantly improves the catalyst separation process (thus cleaning the post-reaction mixture from the catalyst and enabling its reuse) without negatively affecting the colloidal stability of the system. The aspects mentioned above were considered in planning research on new palladium catalysts. In this paper, we focused on studying how the polymeric shell structure influences the complexing capabilities and catalytic properties of the nanosystem. We applied surface-initiated RAFT/MADIX polymerization to introduce the polymeric chain into the surface of magnetic nanoparticles. The application of RAFT polymerization for nanoparticle modification is now broadly investigated because of the good tolerance of RAFT agents to different functional groups, the simplicity of the polymerization process (no catalyst is required), and its stability in water-based systems [42].

Results and discussion

Preparation of core/shell magnetic nanoparticles with a polymeric coating was aimed at the SI-RAFT/MADIX (Surface Initiated Reversible Addition Fragmentation Chain Transfer/Macromolecular Design via Interchange of Xanthates) polymerization technique, which was initiated directly from the surface of the nanoparticles was applied. The surface initiation was enabled by anchoring the chain transfer agent dithiocarbonate onto the nanoparticles (by multistep reactions, i.e., amide bond formation and nucleophilic substitution). This technique was described previously by our team [43, 44]. Synthesized nanohybrids were used to prepare palladium catalysts active in the Heck reaction. In our previous work [14], multistep synthesis anchored the NHC precursor directly on the MNP surface. It is a very efficient method but has a drawback—the amount of ligand embedded in MNP is limited; thus, the number of resulting catalytic centers is also limited. The priorly synthesized system, MNP@NHC-Pd, acted as a suitable catalyst in the Heck reaction; however, because of limited number of active centers, the catalysts needed to be added in high amounts ($\geq$10 mol%). Due to these limitations, the method applying the polymerization reaction presented herein allows the introduction of more ligands on the surface of MNP than previously described. Thus, the prepared catalyst should be active in lower concentration [14].

Ligand synthesis

Complexing ligand 1—imidazolium salt (NHC precursor) was initially synthesized (Fig. 1).

We have chosen NHC precursors due to their excellent stability and ease of synthesis, which makes their production low-cost. Imidazolium salt **1** was synthesized by a substitution reaction of benzyl bromide to imidazole. The original reaction without additives had a meager yield; hence, sodium iodide was added to the reaction mixture. As a result, an NHC precursor (1) with iodide as a counterion was synthesized with a 93% yield. The salt was purified by adding cold ether to the dichloromethane solution to obtain yellowish crystals. X-ray analyses of **1** confirmed the structure of monomer and iodide ion as a counterion (Fig. 1).

Polymerization reactions

Synthesized monomer (imidazolium salt 1) is highly polar, limiting its solubility in most solvents used in the polymerization reaction. The best solubility was observed in methanol; thus, this solvent was chosen for further investigations.

In the polymerization reaction, nanoparticles (Fe_3O_4 nanoparticles) modified by dithiocarbonate groups were used. The synthesis and modification of MNP were described in our previous papers and are presented in Fig. 2 [38, 45]. Shortly, magnetic nanoparticles were precipitated from aqueous solutions of iron chlorides ($FeCl_2{\cdot}4H_2O$ and $FeCl_3{\cdot}6H_2O$) and then covered by siloxane shell (from 3-aminepropyltrimetoxysilane—APTMS). The following two steps

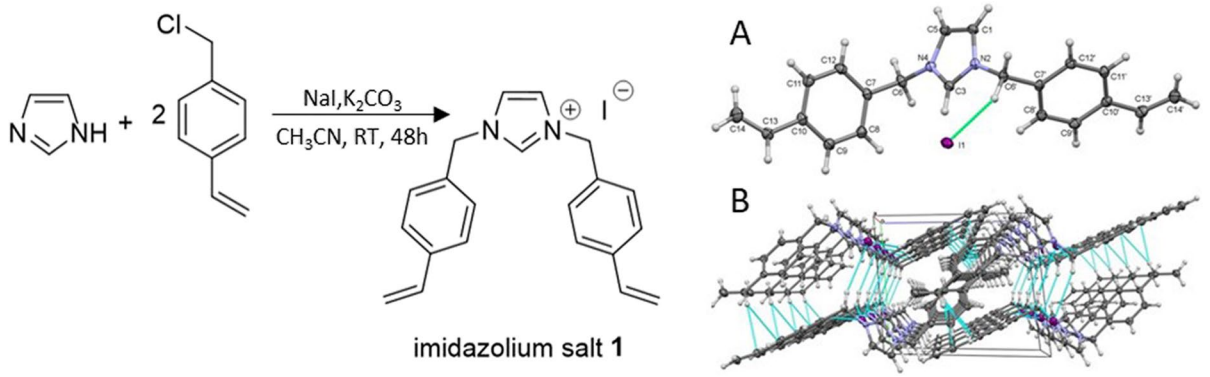

Fig. 1 Synthesis of symmetric imidazolium salt 1 (NHC precursor) active in polymerization reactions (left). **A** The molecular structure of the asymmetric unit of the imidazolium salt 1 showing the atom-labeling scheme and displacement ellipsoids of the non-hydrogen atoms at the 50% probability level—green dashed line depicts one of the C–H…$I^{(-)}$ hydrogen bonds. **B** Non-covalent (blue dashed lines) interactions in its crystal structure

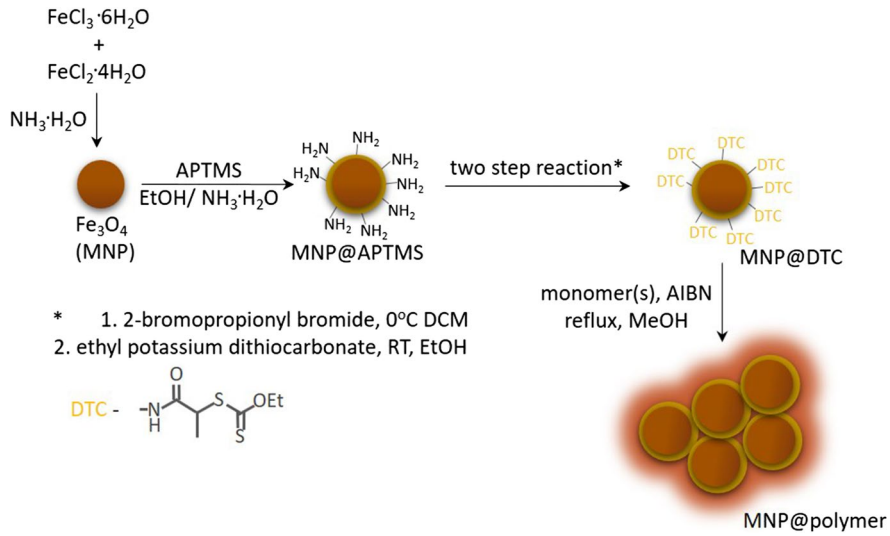

Fig. 2 The preparation of polymer-covered magnetic nanoparticles

led to the preparation of nanoparticles modified by dithiocarbonate (first reaction with 2-bromopropionyl bromide, second with ethyl potassium dithiocarbonate). In the final step, the radical polymerization (RAFT/MADIX) was applied to form a polymeric shell on the magnetic nanoparticles.

Two polymerization strategies were implemented (homopolymerization and random copolymerization) to differentiate the structure of decorated MNP. Homopolymerization creates a polymeric shell (**MNP@PImid**) where ligands are close to each other, which can hinder the accessibility of catalytic centers in the end product (Scheme 1).

For this reason, random copolymerization was performed in the scope of separation of ligand centers. As monomers for random copolymerization, styrene (**MNP@PImid-*r*-PS**) and 1-vinylimidazole (**MNP@PImid-*r*-PVIM**) were chosen (Scheme 1). The polymerization reactions were carried out in methanol or methanol/toluene mixture at boiling point with AIBN as an initiator.

The polymerizable derivative of imidazolium salt was used for a homopolymerization reaction initiated directly from the surface of the nanoparticles; the reaction was carried out at the boiling point of methanol, using AIBN as the initiator. After 24 h of the polymerization reaction, the nanoparticles were separated and washed several times with methanol. After drying the products at 50 °C, they were subjected to

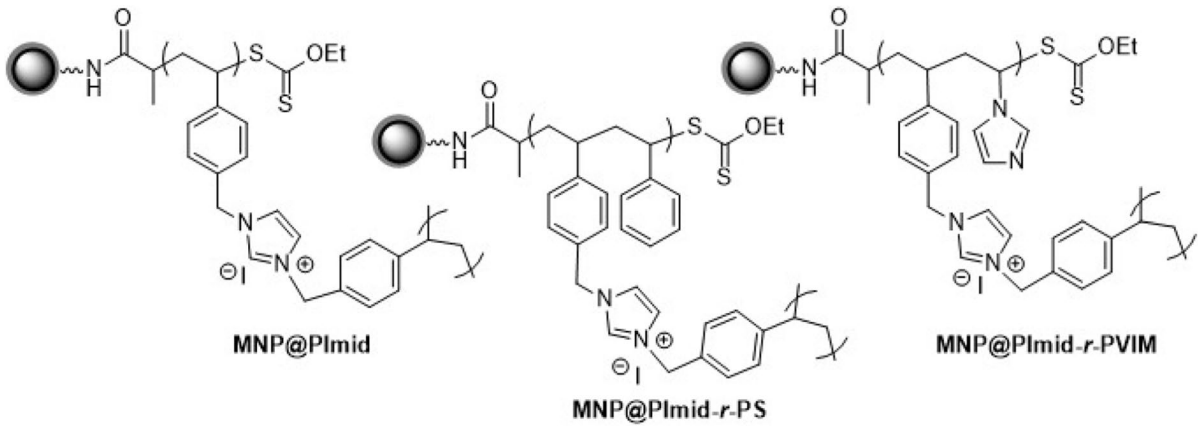

Scheme 1 Nanohybrids obtained by SI-RAFT/MADIX (co)polymerization reactions

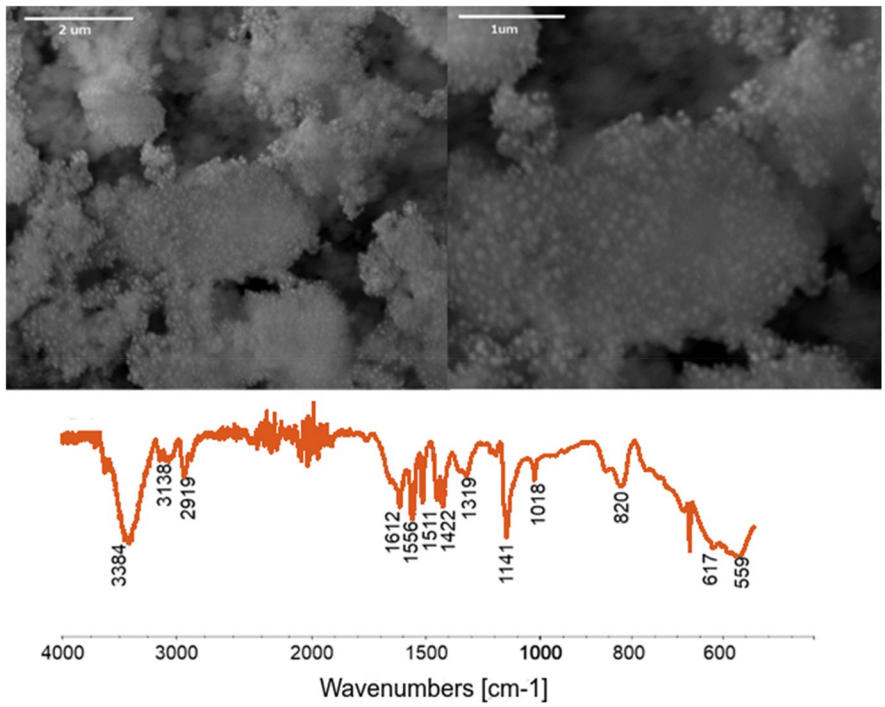

Fig. 3 SEM pictures and FT-IR spectra of MNP@PImid

thermogravimetric and FT-IR analyses (Fig. 3 and Figure S2). In the reaction with imidazolium salt 1 (**MNP@PImid**), large nanoparticle-polymer agglomerates with dimensions of about 100 nm coated with a thick layer of polymer were obtained. The spectroscopic analysis confirmed the presence of poly(imidazolium salt 1) on the surface of the nanoparticles. Figure 3 shows the FT-IR spectrum of MNP@PImid, in which we can observe signals characteristic for the stretching of bonds present in the polymeric shell, i.e., stretching vibrations of aromatic C–H bonds (3138 cm^{-1}), vibrations of aliphatic C–H bonds (2919 cm^{-1}), and vibrations of C–H bonds in the precarbene center (1612 cm^{-1}). Also, signals characteristic of the magnetic core of the nanoparticles are present in the spectra (559 cm^{-1}).

Furthermore, magnetic hybrids with randomly constructed polymeric shells were characterized by FT-IR. As in the case of nanoparticles with

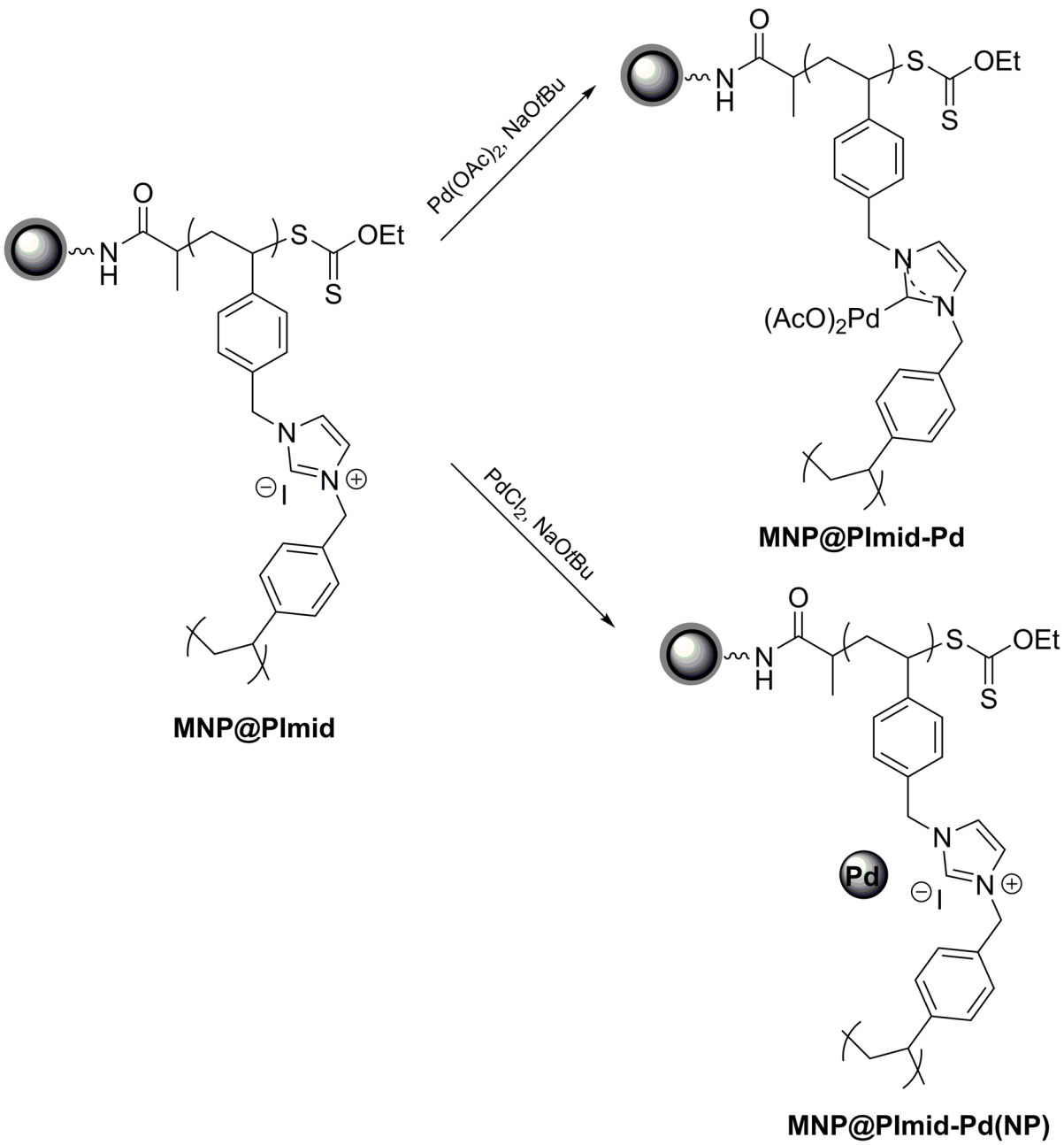

Scheme 2 Creation of palladium complexes using **MNP@PImid** as a ligand

homopolymeric shell (**MNP@PImid**), in the FT-IR spectra of hybrids **MNP@PImid-*r*-PS** and **MNP@PImid-*r*-PVIM**, characteristic signals from the vibrations of bonds present in the polymer chain (C–H at 2900 cm^{-1}) and the polymer side chains (C–H aromatic—signals above 3000 cm^{-1}, C–H in the precarbene center around 1600 cm^{-1}) were observed (Figure S1).

The complexation reactions of palladium

To investigate the influence of the structure of the polymer coating and the palladium salt used in complexation reaction on the complexes formation, magnetic nanoparticles with polymeric shells (**MNP@PImid**, **MNP@Pimid-*r*-PS**, and **MNP@PImid-*r*-PVIM**) and two different palladium ion donors (palladium acetate and palladium

chloride) were used. In Scheme 2, complexation reactions of palladium on **MNP@PImid** are presented.

The **MNP@PImid-Pd** complex was synthesized by using palladium acetate as the metal ion donor and sodium *tert*-butoxide as the base (Scheme 2). Since the polymer coating of the nanoparticles possesses plenty of imidazolium side groups, the palladium complexes with two NHC ligands can be formed in addition to the palladium complexes with one NHC ligand [46]. TEM analyses confirmed that no palladium nanoparticles were created in this case. The application of palladium chloride (as a donor of palladium ions) resulted in obtaining a polymer-inorganic solid phase, covered mainly by palladium nanoparticles **MNP@PImid-Pd(NP)** (Fig. 4).

The above procedures were also used to synthesize palladium complexes with **MNP@PImid-*r*-PS** and **MNP@PImid-*r*-PVIM**. The application of **MNP@PImid-r-PS** led to the production of two palladium catalysts—**MNP@(PImid-Pd)-*r*-PS** was formed in the reaction with palladium acetate. In the reaction with palladium chloride, as in the case of hybrids with a homopolymer structure, palladium nanoparticles bonded to a polymer coating (**MNP@(PImid-Pd(NP))-*r*-PS**) were obtained. Unexpectedly, the application of nanoparticles **MNP@PImid-*r*-PVIM** containing 1-vinylimidazole repeating units led to the formation of palladium nanoparticles on the surface of the solid phase (**MNP@(PImid-Pd(NP))-*r*-PVIM**) in both reactions (using $Pd(OAc)_2$ and $PdCl_2$) (Scheme 3).

The palladium mass content in all five complexes was investigated using the SEM/EDX method. The results are presented in Table 1. In most cases (apart **MNP@(PImid-Pd(NP))-*r*-PVIM**), the highest palladium content was observed in hybrids where palladium nanoparticles are present, e.g., 34 wt% of palladium in **MNP@PImid-Pd(NP)**.

The XRD method was used for the investigation of the presence of palladium in the metallic form on the surface of nanoparticles. The XRD patterns (Fig. 5 and Figure S3) show the presence of a magnetic core (in magnetite/maghemite form) in all investigated particles. The signals from palladium in metallic form were observed in the samples in which Pd nanoparticles were visualized on TEM (the wide peaks informed us that Pd is present in the form of tiny crystals). Moreover, small signals from palladium crystals were also observed in the sample MNP@Pimid-Pd, in which the Pd nanoparticles were not observed in TEM image. It is possible that some of Pd nanoparticles were formed during the Pd anchoring process.

All obtained complexes were used as magnetically separable heterogeneous catalysts in the Heck-type coupling reactions. In the next stage, the differences in the activity and stability of the material differing in the method of palladium bonding on the surface of the solid phase were examined.

The FT-IR and thermogravimetric analysis were used to characterize the obtained polymer-inorganic hybrids. In the spectra of palladium catalysts **MNP@PImid-Pd** and **MNP@(Pimid-Pd)-*r*-PS** (catalysts without the presence of palladium nanoparticles), additional signals at the IR spectra can be observed which were not present in the starting materials (Fig. 6).

Among others, a strong signal coming from the stretching vibrations of the carbonyl group from the acetyl ligand (around 1660 cm^{-1}) was present in the spectra. However, no significant changes were observed

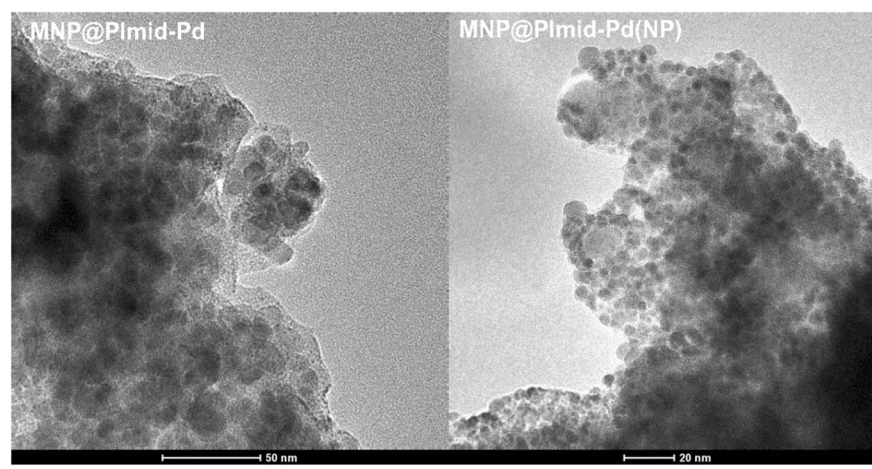

Fig. 4 TEM micrographs of MNP@PImid-Pd (left) and MNP@PImid-Pd(NP) (right)

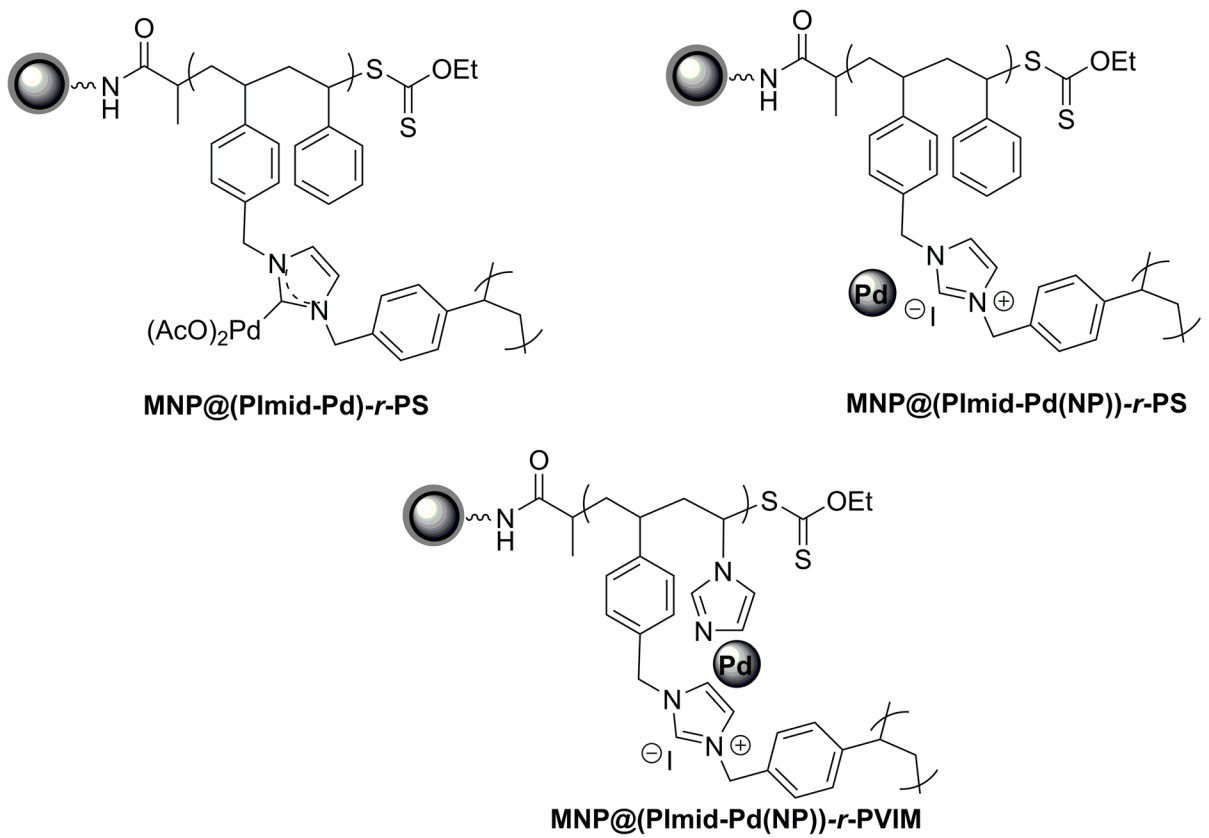

Scheme 3 Proposed structures of palladium complexes obtained from **MNP@PImid-r-PS** and **MNP@PImid-r-PVIM**

Table 1 Palladium % weight content in synthesized hybrids (SEM/EDX)

No	Name	Pd [wt%]
1	MNP@PImid-Pd	18.2
2	MNP@PImid-Pd(NP)	33.9
3	MNP@(PImid-Pd)-*r*-PS	10.8
4	MNP@(PImid-Pd(NP))-*r*-PS	24.3
5	MNP@(PImid-Pd(NP))-*r*-PVIM	5.6

in the signal of the C–H bond vibrations in the precarbene center. It is due to the high thickness of the polymer coating—probably mainly the NHC ligands presented in the outer part of the layer were modified. Less availability of ligands inside the polymeric shell could be induced by cross-linking processes occurred during the polymerization—imidazolium monomer 1 contains two vinyl groups, which cause a cross-linking reaction. Cross-linking could also be the reason for the formation of the agglomerates (approx. 100 nm).

The presence of free NHC carbene precursors was also proved by SEM/EDX investigations, where a decrease in the amount of iodine ions was confirmed. In the FT-IR spectra of hybrids contained palladium nanoparticles (**MNP@PImid-Pd(NP)**, **MNP@(PImid-Pd(NP))-*r*-PS**, **MNP@(PImid-Pd(NP))-*r*-PVIM**), no significant changes were observed in comparison to the starting materials. Only slight shifts of signals originating from the vibrations of bonds that occur in the side chains of polymers were observed.

Magnetic nanoparticles with homopolymer coating (**MNP@PImid**), random copolymeric structure (**MNP@PImid-*r*-PS** and **MNP@PImid-*r*-PVIM**), and their palladium catalysts (**MNP@PImid-Pd**, **MNP@PImid-Pd(NP)**, **MNP@(PImid-Pd)-*r*-PS**, **MNP@(PImid-Pd(NP))-*r*-PS**, **MNP@**

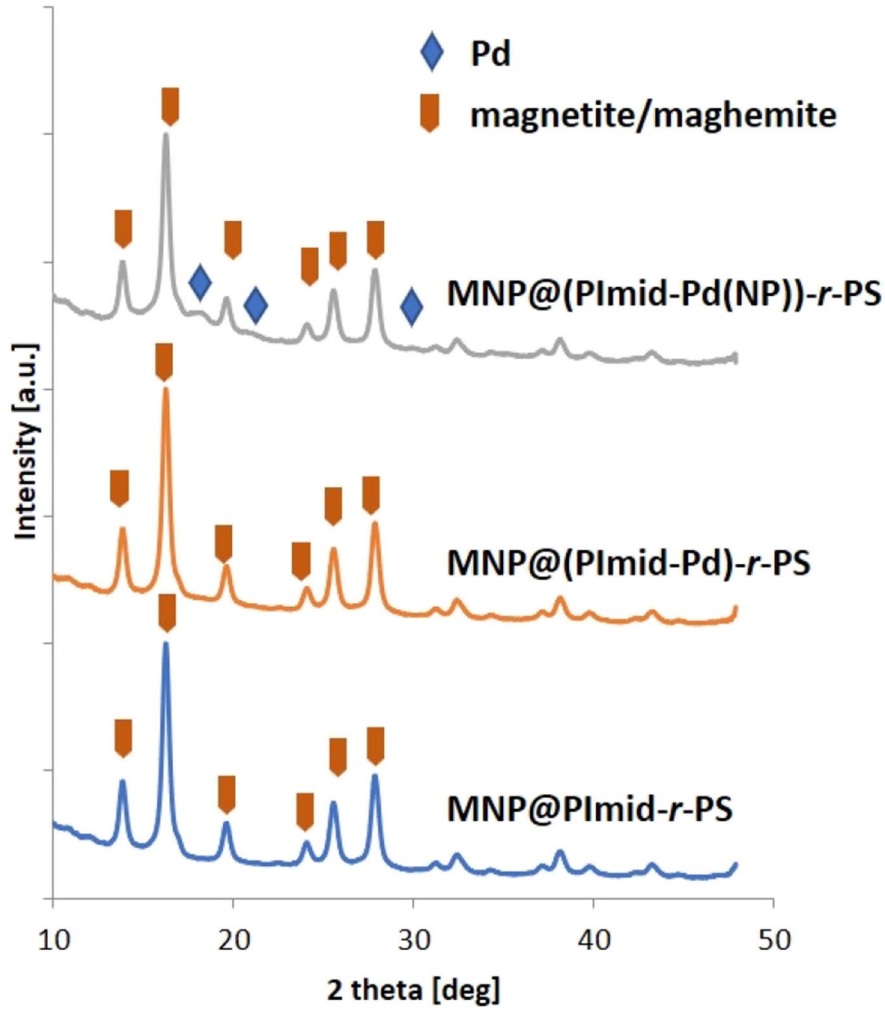

Fig. 5 The XRD patterns of nanoparticles modified by PImid-r-PS polymeric shell and the obtained catalysts

(PImid-Pd(NP))-*r*-PVIM) were characterized by thermogravimetric analysis (Fig. 7 and Figure S4).

In the case of nanoparticles covered with a homopolymer coating (**MNP@PImid**), the weight loss determined from the TG curve was 55%, indicating the formation of a thick polymer coating around at least several nanoparticles, confirmed by TEM analysis. The decomposition of the polymer coating occurred in two stages. The first with a maximum at 466 °C, while the second is in the temperature range from 650 to 790 °C. Palladium catalysts prepared from homopolymer nanoparticles **MNP@PImid-Pd** and **MNP@PImid-Pd(NP)** were also characterized by a two-stage thermal decomposition. The first occurred in a lower temperature range than in the starting material (340–470 °C—the same for both catalysts), and the second in the temperature range from 650 to 790 °C and 650–830 °C for **MNP@PImid-Pd(NP)** and **MNP@PImid-Pd**, respectively. The weight loss was 55% for **MNP@PImid-Pd** and 44% for **MNP@PImid-Pd(NP)**. Apparent differences in thermal decomposition between the palladium complexes and the starting material testify to the chemical modification of the polymer surface. A lower degree of decomposition of the **MNP@PImid-Pd(NP)** than **MNP@PImid** indicates the presence of palladium residues, which are indecomposable at the measurement temperature. What seems surprising is the course of the decay curve of complex **MNP@PImid-Pd**, in which, despite the presence of palladium in the structure, we observed the same weight loss as in the starting material (**MNP@PImid**). The Pd ion complexation process can explain this fact. While the NHC-Pd complex is formed, an iodide ion

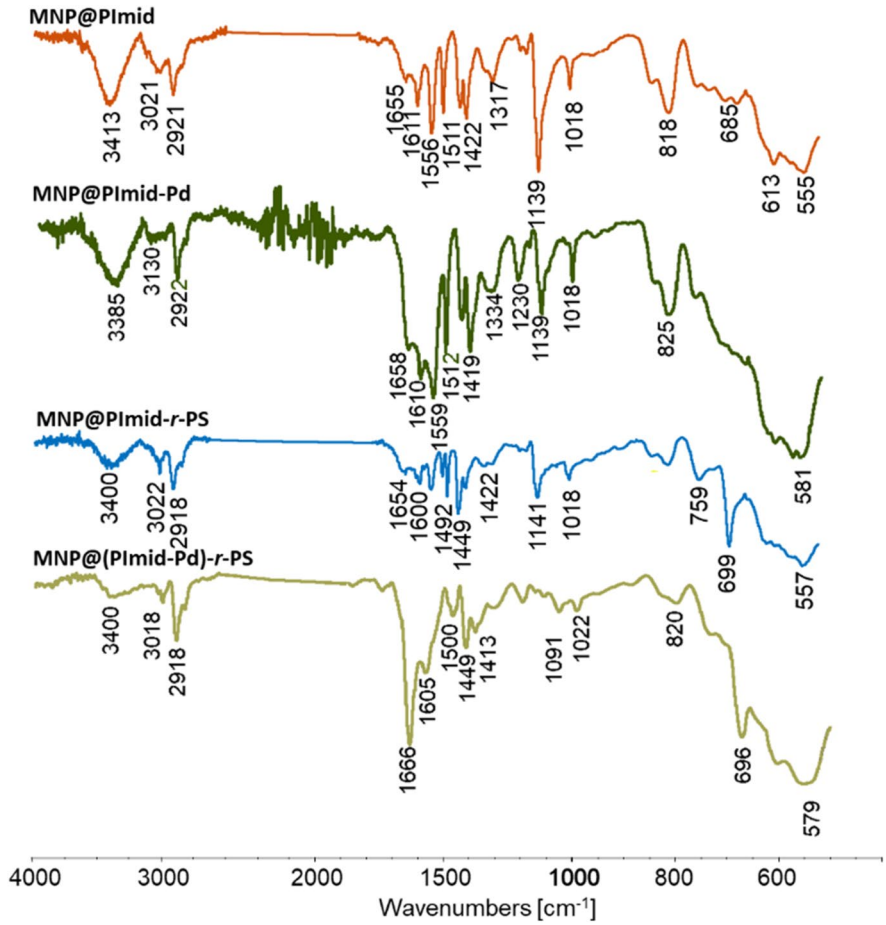

Fig. 6 FT-IR spectra of palladium complexes of hybrids covered by the shell with homo- and copolymeric structure

is produced as a by-product, which is washed out during purification.

Consequently, the percentage of the degradable part (at a specified temperature) increases. However, we do not observe an increase in weight loss because it is compensated by palladium, which does not degrade under these conditions. Nanoparticles with copolymer coatings (**MNP@PImid-*r*-PS** and **MNP@PImid-*r*-PVIM**) and their palladium complexes degrade similarly to nanoparticles with a homopolymer coating. The decomposition data of polymer-inorganic hybrids are summarized in Table S4. A low percentage of weight loss in the case of nanoparticles covered with a copolymer coating with a gradient structure comprised of *N*-vinylimidazole units (compared to magnetic carriers **MNP@PImid** and **MNP@PImid-*r*-PS**) indicates the formation of a thin polymer coating (confirmed by TEM). Formation of the thin polymeric layer is caused by the low reactivity of 1-vinylimidazole in controlled radical polymerization reactions [47, 48]—1-vinylimidazole is categorized as the non-stabilized monomer (i.e., LAM—less activated monomers) which favor non-controlled polymerization [49]. In our case, the most probable scenario was that polymerization of 1-vinylimidazole occurred mainly in suspension rather than at magnetic nanoparticle surfaces. Nevertheless, in the reaction mixture, imidazolium salt 1 monomer was also present, and its polymerization on the surface of MNP was also limited (compared to **MNP@Pimid** hybrids). It appears that the competition between polymerization reaction of imidazolium salt 1 on magnetic nanoparticles and in solution is shifted toward polymerization in solution because of presence of 1-vinylimidazole.

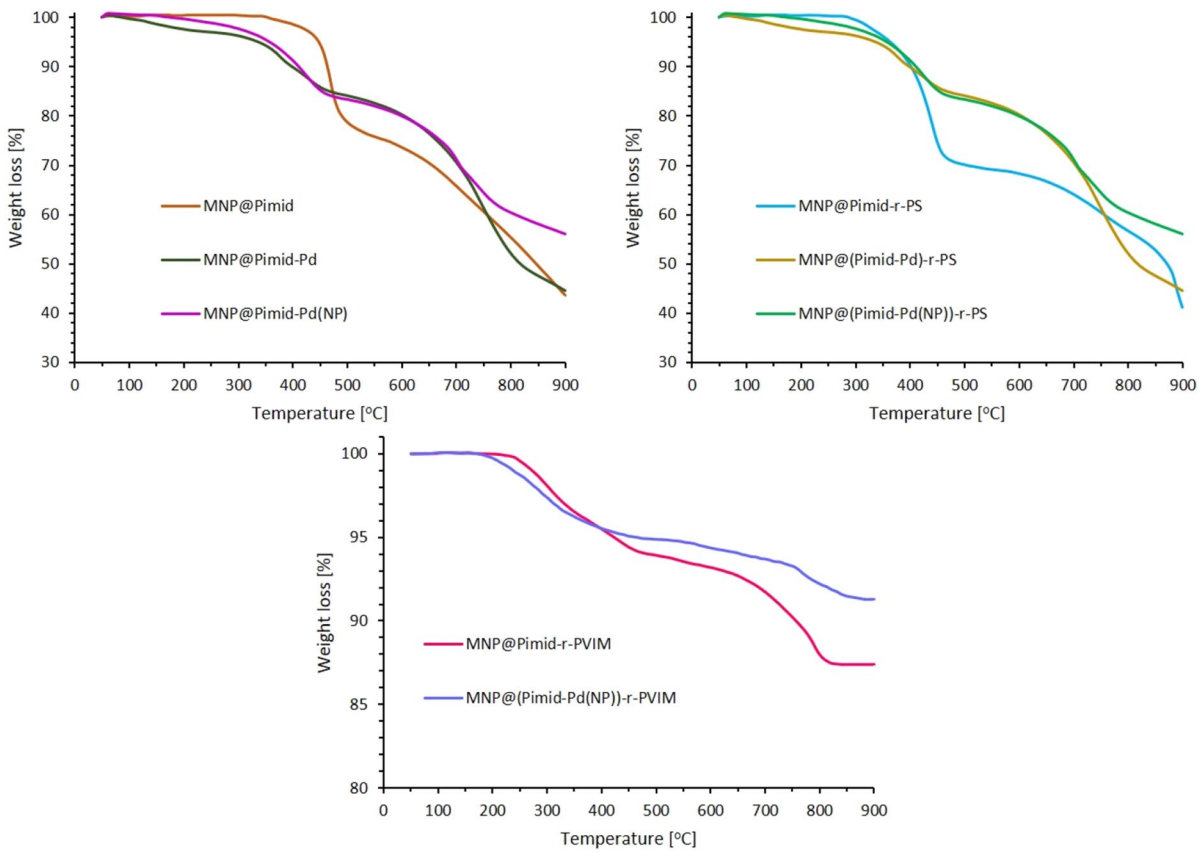

Fig. 7 Thermal analyses of magnetic nanoparticles with homopolymeric and copolymeric shells and their Pd complexes

The catalytic activity of obtained polymer-inorganic hybrids—palladium complexes

The activity of the obtained palladium catalysts was tested in the Heck-type C–C coupling reaction—in the reaction of iodobenzene with *n*-butyl acrylate. Palladium catalysts (**MNP@Pimid-Pd**, **MNP@PImid-Pd(NP)**, **MNP@(PImid-Pd)-*r*-PS**, **MNP@(Pimid-Pd(NP))-*r*-PS**, and **MNP@(Pimid-Pd(NP))-*r*-PVIM**) were used in an amount of 1 mol%. The reactions were carried out for 3 h in DMF at 140 °C. The results are presented in Fig. 8.

The best results were obtained when catalysts **MNP@PImid-Pd** and **MNP@PImid-Pd(NP)-*r*-PVIM** were used. The yields of the Heck reaction were 52% (TON = 52, TOF = 0.28) and 56% (TON = 56, TOF = 0.31), respectively. The remaining catalysts were characterized by poor catalytic activity, and the obtained reaction yields did not exceed 40%. For this reason, it was decided to use only the catalysts mentioned above for further research. To improve the efficiency of the reaction of iodobenzene with the butyl acrylate, 10 mol% of catalysts was used. In the case of **MNP@PImid-Pd**, the efficiency increased by 12 percentage points (yield = 64%, TON = 6.4, TOF = 0.035), while increasing the addition of **MNP@PImid-Pd(NP)-*r*-PVIM** resulted in a decrease in its activity (the efficiency decreased from 56 to 41%, TON = 4.1, TOF = 0.022). It is probably related to the aggregation of the **MNP@PImid-Pd(NP)-*r*-PVIM** that occurs under these conditions and leads to reduced accessibility of the catalytically active sites. Such aggregation was not observed in the case of **MNP@PImid-Pd**. It could be related to the large thickness of the polymer coating surrounding the magnetic core, which reduces the strength of the magnetic interactions between the individual particles.

Additionally, the lower efficiency of **MNP@PImid-Pd(NP)-*r*-PVIM** catalyst can be caused by

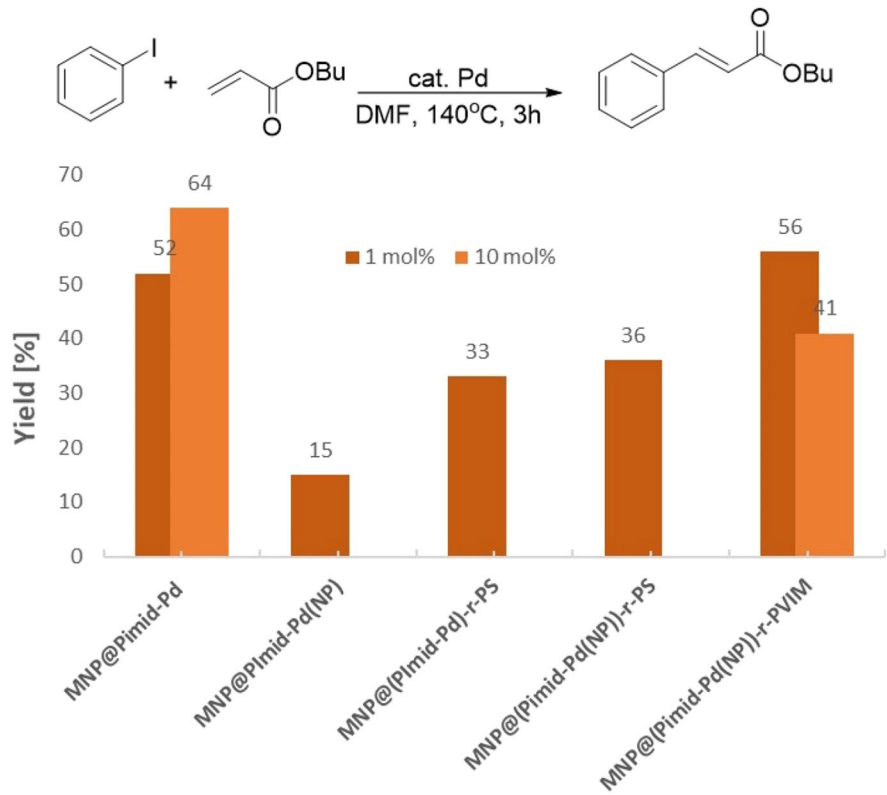

Fig. 8 Scheme of model Heck reaction and the catalytic test results for all hybrids containing palladium 1 mol% and 10 mol%

solid phase influence on the effectiveness of the anchored catalyst. In Heck reactions performed with **MNP@Pimid-Pd** catalyst, the amount of solid phase used was 3 times lower than in the case of **MNP@PImid-Pd(NP)-*r*-PVIM** (the added amount of the catalyst was calculated on the mass content of palladium presented on a solid phase). These two factors lowered the effectiveness of the catalytic activity of the **MNP@PImid-Pd(NP)-*r*-PVIM** catalyst.

After the Heck reaction, the catalysts were separated, washed, and dried. The catalysts were recovered in 80%. The recovered material was subjected to SEM/EDX analysis to determine if the palladium content changed after the reaction. In each case, a decrease in the palladium content was observed (Fig. 9).

The most significant decrease in palladium content was observed when this metal was bound to a solid phase in the form of nanoparticles—catalysts **MNP@PImid-Pd(NP)**, **MNP@(PImid-Pd(NP))-*r*-PS**, and **MNP@(PImid-Pd(NP))-*r*-PVIM**. The palladium content in these hybrids decreased by 79% (both in the case of catalyst **MNP@PImid-Pd(NP)** and **MNP@(PImid-Pd(NP))-*r*-PS**) and by 83% in the case of catalyst **MNP@(PImid-Pd(NP))-*r*-PVIM**. A minor decrease in palladium content was observed while examining complexes MNP@PImid-Pd and **MNP@(PImid-Pd)-*r*-PS** (the Pd content decreased by 44 and 36%, respectively). The results conclude that catalysts containing palladium in the form of nanoparticles are less stable (palladium nanoparticles are poorly bound to the polymer coating—palladium quickly gets into the reaction mixture) compared to those with palladium bonded directly to the ligand. Due to the highest activity of catalysts **MNP@PImid-Pd** and **MNP@(PImid-Pd(NP))-*r*-PVIM** during the first use, it was decided to investigate their recyclability in the Heck reaction. The 1 mol% of catalysts were used to examine the model reaction of iodobenzene with butyl acrylate.

The activity of **MNP@(PImid-Pd(NP))-*r*-PVIM** decreased significantly, and the product was obtained in only 3% yield, while complex **MNP@PImid-Pd** was still active in this reaction, although the obtained yield also reduced (from 52 to 44%) (Fig. 10).

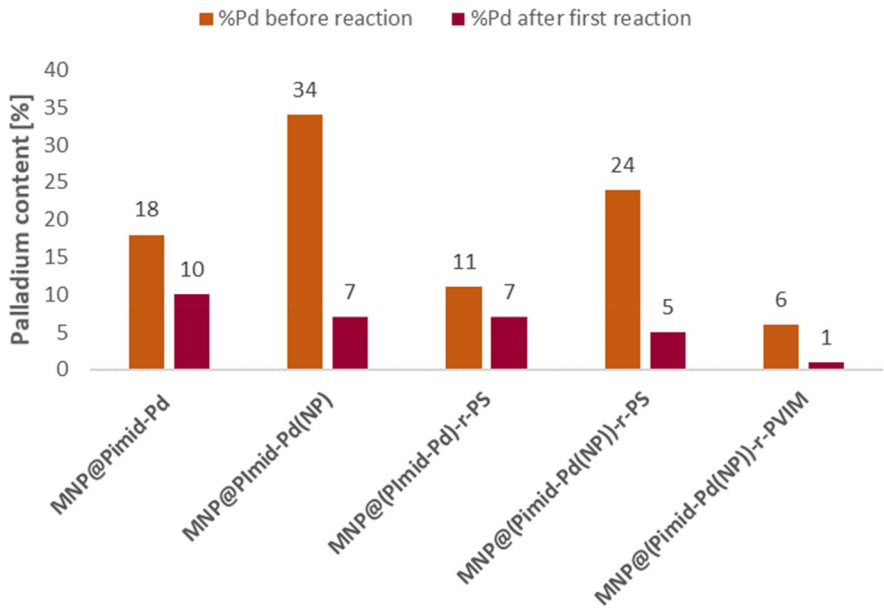

Fig. 9 The palladium content investigation results (SEM/EDX)

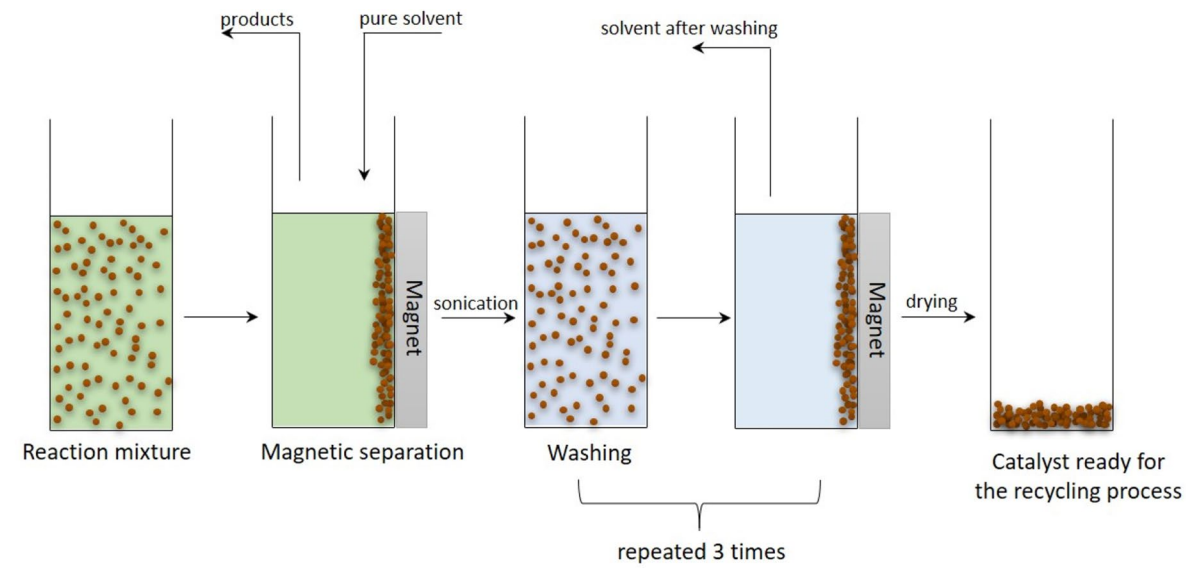

	1st use	2nd use
MNP@(PImid-Pd(NP))-*r*-PVIM	56%	3%
MNP@PImid-Pd	52%	44%

Fig. 10 Graphical representation of the catalyst purification process before recycling tests (up) and the reaction yields with the recycled catalysts (bottom)

Conclusions

In conclusion, magnetic nanoparticles with polymeric coatings of various structures were synthesized using three monomers: NHC carbene precursor (imidazolium salt 1), styrene, and 1-vinylimidazole. SI-RAFT/MADIX polymerization was used to construct a polymer coating on the surface of magnetic nanoparticles.

Synthesis of dithiocarbonates due to modification of aminosiloxane groups of nanoparticles allowed the growth of polymer chains directly from their surface (SI-RAFT/MADIX). In addition, this technique enables the creation of copolymers and thus provides a broad spectrum of possibilities for creating polymer coatings of various compositions. The activity of the obtained palladium catalysts was tested in the Heck-type C–C coupling reaction. Different physicochemical methods were used to characterize the obtained catalysts. The most active catalyst was achieved when the complex was attached to magnetic nanoparticles due to the homopolymerization of symmetric imidazolium salt 1 (**MNP@PImid-Pd**). Applying 1-vinylimidazole or styrene as comonomers in random copolymerization influences the catalytic activity of obtained catalysts. The average catalytic efficiency of produced catalysts may be caused not only by the structure of the polymer-inorganic phase or the method of catalyst immobilization on the hybrid surface but also by the activity of the complex itself [50]. It was also shown that catalysts containing palladium nanoparticles on the surface of nanoparticles are less stable, and their activity significantly decreases when reused.

Materials and methods

Acetonitrile (HPLC grade, Aldrich), 3-aminopropyltrimetoxysilane (98%, Aldrich), 2,2′-azobis(2-methylpropionitrile)—AIBN (95%, MERCK), butyl acrylate (98%, Aldrich), carbon disulfide (99.9%, Aldrich), imidazole (98%, Fluka), iodobenzene (98%, Aldrich), iron (II) chloride tetrahydrate (98%, Aldrich), iron (III) chloride hexahydrate (99%, Aldrich), palladium (II) acetate (99.9%, Aldrich), palladium (II) chloride (99.9%, Aldrich), sodium iodide (99.5%, Aldrich), styrene (99.9%, Aldrich), 4-vinylbenzyl chloride (98%, Aldrich), 1-vinylimidazole (99%, Aldrich).

Aqueous ammonia, DMF, Et_3N, K_2CO_3, KOH, and MeOH were purchased from Avantor Performance Materials Poland S.A.

Transmission electron microscope

Tecnai G2 X-Twin microscope was used to take images at the accelerating 200 kV voltage. Samples for TEM were prepared on holey carbon copper grids.

Energy-dispersive X-ray spectroscopy (EDX)

EDX analyses were collected from the samples imaged by scanning electron microscope (SEM) (TFP 2017/12 Inspect S50 FEI)—detector Ametek Octane Pro. Samples for SEM microscopy were prepared on aluminum tables.

X-ray powder diffraction (XRD)

Room temperature XRD measurements were performed using Empyrean PANalytical powder diffractometer.

Nuclear magnetic resonance (NMR)

1H and 13C spectra were recorded on Bruker Avance II 400 spectrometer operating at 400 and 100 MHz, respectively.

Attenuated total reflectance Fourier-transform infrared spectroscopy (ATR-FTIR)

Spectra were made on Thermo Scientific Nicolet 6700 FTIR spectrophotometer, possessing ATR accessory. Spectra were collected in the wavenumber range from 4000 to 500 cm^{-1} by adding 32 scans with a resolution of 4 cm^{-1}.

Thermogravimetric analysis (TGA)

Thermogravimetric analyses were done using a Mettler Toledo Star TGA/DSC unit. Samples weighing 2–3 mg were placed in aluminum oxide crucibles and heated from 50 to 900 °C. The heating rate was equal to 10 K min^{-1}, and an argon flow rate was 40 mL/min.

Crystallographic data (XRD)

Crystallographic data (XRD) were collected on the Oxford Diffraction SuperNova DualSource diffractometer using the monochromated Cu Kα X-ray source (λ = 1.54184). The crystals were kept at 100 K during data collection. Data reduction and analytical absorption correction were performed with CrysAlis PRO [51] using Olex2 [52]. The structure was solved with the ShelXS [53] structure solution program using direct methods and refined with the

ShelXL [53] refinement package using least squares minimization.

Experimental section

General procedure for MNP synthesis and their modification

The procedure for magnetic nanoparticle synthesis and their further modifications was previously described in our work [45].

SI-RAFT polymerization reaction procedures

MNP coated with 1,3-bis(4-vinylbenzyl)-1H-imidazol-3-ium iodide polymer—**MNP@PImid.**

Dithiocarbonate-modified nanoparticles (50 mg) were sonically dispersed in methanol (1 mL). Subsequently, the 1,3-bis(4-vinylbenzyl)-1H-imidazol-3-ium iodide (100 mg) and AIBN (9 mg) were added. The mixture was refluxed for 20 h. The initiator was added in three portions at the beginning and after 2 and 4 h of stirring (3 × 3 mg). The nanoparticles were separated from the reaction mixture by the external magnetic field and then washed three times with methanol and once with dichloromethane. Nanoparticles were dried overnight at 60°. ATR FT-IR (cm^{-1}): 3427, 3052, 2923, 1613, 1556, 1448, 1143, 581.

MNP coated with 1,3-bis(4-vinylbenzyl)-1H-imidazol-3-ium iodide and styrene/1-vinylimidazole random copolymers—**MNP@PImid-*r*-PS** and **MNP@PImid-*r*-PVIM.**

Dithiocarbonate-modified nanoparticles (50 mg) were sonically dispersed in methanol (1 mL). Subsequently, the 1,3-bis(4-vinylbenzyl)-1H-imidazol-3-ium iodide (50 mg), styrene/1-vinylimidazole (86 mg), and AIBN (12 mg) were added. The mixture was refluxed for 24 h. The initiator was added in four portions at the beginning after 2, 4, and 16 h of stirring (4 × 3 mg). The nanoparticles were separated from the reaction mixture by an external magnetic field and then washed three times with ethanol and once with dichloromethane. Nanoparticles were dried overnight at 60 °C.

MNP@PImid-*r*-PS ATR FT-IR (cm^{-1}): 3387, 3012, 2924, 1646, 1558, 1450, 1024, 553.

MNP@PImid-*r*-PVIM ATR FT-IR (cm^{-1}): 3427, 3052, 2923, 1613, 1556, 1448, 1143, 581.

1,3-Bis(4-vinylbenzyl)-1H-imidazolium iodide

Imidazole (1.47 mmol, 1 eq), dried K_2CO_3 (3.08 mmol, 2.1 eq), and KI (3.08 mmol, 2.1 eq) were put in a round-bottomed flask, then freshly distilled acetonitrile (5 mL) was added. The mixture was stirred for 30 min, and subsequently, the 4-vinylbenzyl chloride (2.94 mmol, 2 eq) dissolved in 5 mL of acetonitrile was slowly added to the reaction mixture. The mixture was stirred under an inert atmosphere at room temperature for 48 h. The reaction mixture was protected against light. Subsequently, the solvent was evaporated, and water was added to the mixture. It was purified by extraction (three times with dichloromethane). The organic layers were combined and dried with anhydrous Na_2SO_4. The mixture was filtered, and the filtrate was evaporated. The crude product was washed with cyclohexane and diethyl ether. The residue was then dissolved in dichloromethane and precipitated by an excess of diethyl ether. The pure product was obtained with a yield of 61%.

^{1}H NMR (δ, ppm, $CDCl_3$): 10.33 (s, 1H), 7.46 (d, 4H, J = 8.16 Hz), 7.39 (d, 4H, J = 8.16 Hz), 7.27 (s, 4H), 6.62–6.69 (dd, 2H, J1 = 10.92 Hz, J2 = 17.60 Hz), 5.74 (d, 2H, J = 17.60), 5.53 (s, 4H), 5.29 (d, 2H, J = 10.88 Hz).

^{13}C NMR (δ, ppm, $CDCl_3$): 138.9 ($2 \times C_{IV}$), 136.3 (C_{III}), 135.7 ($2 \times C_{III}$), 131.7 ($2 \times C_{IV}$), 129.4 ($4 \times C_{III}$), 127.2 ($4 \times C_{III}$), 121.9 ($2 \times C_{III}$), 115.5 ($2 \times C_{II}$), 53.3 ($2 \times C_{II}$).

ATR-FTIR (cm^{-1}): 3121, 2963, 1550, 1444, 1137.

General procedure for Heck reaction

The palladium catalyst (1 or 10 mol%) was ultrasonically dispersed in freshly distilled DMF (1 mL). Then, $NaHCO_3$ (0.1 mmol), iodobenzene (0.15 mmol), and butyl acrylate (0.1 mmol) were added. The mixture was stirred under reflux for 3 h, then cooled, and the catalyst was separated from the reaction mixture using an external magnetic field (Nd magnet). The reaction mixture was extracted with diethyl ether (3 times). Organic layers were collected and dried under Na_2SO_4 (anhydrous). Next, the solvent was evaporated, and the residue was purified on silica gel (eluent—hexane).

Acknowledgements The authors are thankful for Dr. Leszek Siergiejczyk for NMR spectra and Dr. hab. Beata Kalska-Szostko for powder XRD measurements.

Author contribution IMT: conceptualization (lead), founding acquisition, investigation (lead), methodology, project administration (equal), visualization, writing—original draft preparation, writing—review and editing (equal). SW: investigation (supporting—diffraction). AZW: investigation (supporting—TGA), conceptualization (supporting), project administration (equal), writing—review and editing (equal), supervision.

Funding This work was financially supported by the National Science Centre, Poland, grant No. NCN/2016/21/B/ST5/01316 (IMT). The analyses were performed in the Centre of Synthesis and Analysis BioNanoTechno of the University of Bialystok. The equipment in the Centre was funded by the EU as part of the Operational Program Development of Eastern Poland 2007–2013, projects POPW.01.03.00–20-034/09–00 and POPW.01.03.00–20-004/11.

Data availability The data that support the findings of this study are available on request from the corresponding author [IMT].

Declarations

Competing interests The authors declare no competing interests.

Ethical approval Not applicable.

Conflict of interest There are no conflicts to declare.

References

1. Shylesh S, Schünemann V, Thiel WR (2010) Magnetically separable nanocatalysts: bridges between homogeneous and heterogeneous catalysis. Angew Chem Int Ed 49:3428–3459. https://doi.org/10.1002/anie.200905684
2. Wang D, Astruc D (2014) Fast-growing field of magnetically recyclable nanocatalysts. Chem Rev 114:6949–6985. https://doi.org/10.1021/cr500134h
3. Miceli M, Frontera P, Macario A, Malara A (2021) Recovery/reuse of heterogeneous supported spent catalysts. Catalysts 11:591. https://doi.org/10.3390/catal11050591
4. Schubert J, Chanana M (2018) Coating matters: review on colloidal stability of nanoparticles with biocompatible coatings in biological media, living cells and organisms. Curr Med Chem 25:4553–4586. https://doi.org/10.2174/0929867325666180601101859
5. Almahfood M, Bai B (2018) The synergistic effects of nanoparticle-surfactant nanofluids in EOR applications. J Pet Sci Eng 171:196–210. https://doi.org/10.1016/j.petrol.2018.07.030
6. Shon YS, Choi D (2007) Dendritic functionalization of metal nanoparticles for nanoparticle-cored dendrimers. Curr Nanosci 3:245–254. https://doi.org/10.2174/157341307781422997
7. He Z, Alexandridis P (2017) Ionic liquid and nanoparticle hybrid systems: emerging applications. Adv Colloid Interface Sci 244:54–70. https://doi.org/10.1016/j.cis.2016.08.004
8. Avirdi E, Hooshmand SE, Sepahvand H, Vishwanathan V, Bahadur I, Katata-Seru LM, Varma RS (2022) Ionic liquids-assisted greener preparation of silver nanoparticles. Curr Opin Green Sustain Chem 33:100581. https://doi.org/10.1016/j.cogsc.2021.100581
9. He Z, Alexandridis P (2015) Nanoparticles in ionic liquids: interactions and organization. Phys Chem Chem Phys 17:18238–18261. https://doi.org/10.1039/C5CP01620G
10. Liu G, Gao J, Ai H, Chen X (2013) Applications and potential toxicity of magnetic iron oxide nanoparticles. Small 9:1533–1545. https://doi.org/10.1002/smll.201201531
11. Ahmad T, Phul R, Khan H (2019) Iron oxide nanoparticles: an efficient nano-catalyst. Curr Org Chem 23:994–1004. https://doi.org/10.2174/1385272823666190314153208
12. Sangaiya P, Jayaprakash R (2018) A review on iron oxide nanoparticles and their biomedical applications. J Supercond Nov Magn 31:3397–3413. https://doi.org/10.1007/s10948-018-4841-2
13. Misztalewska-Turkowicz I, Markiewicz KH, Michalak M, Wilczewska AZ (2018) NHC-copper complexes immobilized on magnetic nanoparticles: synthesis and catalytic activity in the CuAAC reactions. J Catal 362:46–54. https://doi.org/10.1016/j.jcat.2018.03.015
14. Wilczewska AZ, Misztalewska I (2014) Direct synthesis of imidazolinium salt on magnetic nanoparticles and its palladium complex application in the heck reaction. Organometallics 33:5203–5208. https://doi.org/10.1021/om500507q
15. Arduengo AJ III, Harlow RL, Kline M (1991) A stable crystalline carbene. J Am Chem Soc 113:361–363
16. Ranganath KVS, Onitsuka S, Kumar AK, Inanaga J (2013) Recent progress of N-heterocyclic carbenes in heterogeneous catalysis. Catal Sci Technol. https://doi.org/10.1039/c3cy00118k
17. Ortuño MA, López N (2019) Reaction mechanisms at the homogeneous–heterogeneous frontier: insights from first-principles studies on ligand-decorated metal nanoparticles. Catal Sci Technol 9:5173–5185. https://doi.org/10.1039/C9CY01351B
18. Koy M, Bellotti P, Das M, Glorius F (2021) N-heterocyclic carbenes as tunable ligands for catalytic metal surfaces. Nat Catal 4:352–363. https://doi.org/10.1038/s41929-021-00607-z
19. Cerezo-Navarrete C, Lara P, Martínez-Prieto LM (2020) Organometallic nanoparticles ligated by NHCs: synthesis, surface chemistry and ligand effects. Catalysts 10:1144. https://doi.org/10.3390/catal10101144
20. Ashraf M, Ahmad MS, Inomata Y, Ullah N, Tahir MN, Kida T (2023) Transition metal nanoparticles as nanocatalysts for Suzuki, Heck and Sonogashira cross-coupling

reactions. Coord Chem Rev 476:214928. https://doi.org/10.1016/j.ccr.2022.214928
21. Piermatti O (2021) Green synthesis of Pd nanoparticles for sustainable and environmentally benign processes. Catalysts 11:1258. https://doi.org/10.3390/catal11111258
22. Gebre SH (2023) Recent developments of supported and magnetic nanocatalysts for organic transformations: an up-to-date review. Appl Nanosci 13:15–63. https://doi.org/10.1007/s13204-021-01888-3
23. De Tovar J, Rataboul F, Djakovitch L (2021) Heterogenization of Pd(II) complexes as catalysts for the Suzuki-Miyaura reaction. Appl Catal Gen 627:118381. https://doi.org/10.1016/j.apcata.2021.118381
24 Bourouina A, Meille V, de Bellefon C (2019) About solid phase vs. liquid phase in Suzuki-Miyaura reaction. Catalysts 9(1):60. https://doi.org/10.3390/catal9010060
25. Maleki A, Taheri-Ledari R, Ghalavand R, Firouzi-Haji R (2020) Palladium-decorated o-phenylenediamine-functionalized Fe3O4/SiO2 magnetic nanoparticles: a promising solid-state catalytic system used for Suzuki-Miyaura coupling reactions. J Phys Chem Solids 136:109200. https://doi.org/10.1016/j.jpcs.2019.109200
26. Maleki A, Taheri-Ledari R, Ghalavand R (2020) Design and fabrication of a magnetite-based polymer-supported hybrid nanocomposite: a promising heterogeneous catalytic system utilized in known palladium-assisted coupling reactions. Comb Chem High Throughput Screen 23:119–125. https://doi.org/10.2174/1386207323666200128152136
27. Khabibullin A, Mastan E, Matyjaszewski K, Zhu S (2015) Surface-initiated atom transfer radical polymerization. In: Vana P (ed) Controlled radical polymerization at and from solid surfaces. Springer International Publishing, Cham, pp 29–76
28. Mocny P, Klok H-A (2020) Complex polymer topologies and polymer—nanoparticle hybrid films prepared via surface-initiated controlled radical polymerization. Prog Polym Sci 100:101185. https://doi.org/10.1016/j.progpolymsci.2019.101185
29. Gholinejad M, Mozafari S, Nikfarjam N, Nayeri S, Sansano JM (2023) Bimetallic AuCo supported on magnetic crosslinked copoly(ionic liquid) nanohydrogel and study of its catalytic activity. Appl Organomet Chem 37:e7223. https://doi.org/10.1002/aoc.7223
30. Gholinejad M, Afrasi M, Nikfarjam N, Nájera C (2018) Magnetic crosslinked copoly(ionic liquid) nanohydrogel supported palladium nanoparticles as efficient catalysts for the selective aerobic oxidation of alcohols. Appl Catal Gen 563:185–195. https://doi.org/10.1016/j.apcata.2018.07.009
31. Kohestanian M, Pourjavadi A, Keshavarzi N (2022) Facile and tunable method for polymeric surface modification of magnetic nanoparticles via RAFT polymerization: preparation, characterization, and drug release properties. Eur Polym J 167:111067. https://doi.org/10.1016/j.eurpolymj.2022.111067
32. Nasrollahzadeh M, Sajjadi M, Shokouhimehr M, Varma RS (2019) Recent developments in palladium (nano)catalysts supported on polymers for selective and sustainable oxidation processes. Coord Chem Rev 397:54–75. https://doi.org/10.1016/j.ccr.2019.06.010
33. Vaino AR, Janda KD (2000) Solid-phase organic synthesis: a critical understanding of the resin. J Comb Chem 2:579–596. https://doi.org/10.1021/cc000046o
34. Ghasemi S, Badri F, Rahbar Kafshboran H (2023) Pd catalyst supported thermo-responsive modified poly(N-isopropylacrylamide) grafted Fe3O4@CQD@Si in Heck coupling reaction. Asian J Green Chem. https://doi.org/10.48309/ajgc.2024.408188.1401
35. Yang Y, Zhu W, Shi B, Lü C (2020) Construction of a thermo-responsive polymer brush decorated Fe_3O_4@catechol-formaldehyde resin core–shell nanosphere stabilized carbon dots/PdNP nanohybrid and its application as an efficient catalyst. J Mater Chem A 8:4017–4029. https://doi.org/10.1039/C9TA12614G
36. Tabatabaei Rezaei SJ, Shamseddin A, Ramazani A, Mashhadi Malekzadeh A, Azimzadeh Asiabi P (2017) Palladium nanoparticles immobilized on amphiphilic and hyperbranched polymer-functionalized magnetic nanoparticles: an efficient semi-heterogeneous catalyst for Heck reaction. Appl Organomet Chem 31:e3707. https://doi.org/10.1002/aoc.3707
37. Veisi H, Sarachegol P, Hemmati S (2018) Palladium(II) anchored on polydopamine coated-magnetic nanoparticles (Fe3O4@PDA@Pd(II)): a heterogeneous and core–shell nanocatalyst in Buchwald-Hartwig C-N cross coupling reactions. Polyhedron 156:64–71. https://doi.org/10.1016/j.poly.2018.09.019
38. Misztalewska-Turkowicz I, Maj J, Leśniewska B, Wojtulewski S, Zgłobicka I, Wilczewska AZ (2023) Polymer-covered magnetic nanoparticles as a palladium Pickering interfacial catalyst for the Suzuki-Miyaura reaction performed in a water environment. J Phys Chem C 127:19937–19946. https://doi.org/10.1021/acs.jpcc.3c02598
39. Zhou D, Zhu L-W, Wu B-H, Xu Z-K, Wan L-S (2022) End-functionalized polymers by controlled/living radical polymerizations: synthesis and applications. Polym Chem 13:300–358. https://doi.org/10.1039/D1PY01252E
40. Bräse S, Lauterwasser F, Ziegert RE (2003) Recent advances in asymmetric C-C and C-heteroatom bond forming reactions using polymer-bound catalysts. Adv Synth Catal 345:869–929. https://doi.org/10.1002/adsc.200202164
41. Nguyen TPT, Ménager C, Rieger J, Coumes F (2023) Rational design of stimuli-responsive magnetic polymer hybrid (nano)materials. Polym Int 72:899–919. https://doi.org/10.1002/pi.6510
42. Peng W, Cai Y, Fanslau L, Vana P (2021) Nanoengineering with RAFT polymers: from nanocomposite design to applications. Polym Chem 12:6198–6229. https://doi.org/10.1039/D1PY01172C
43. Wilczewska AZ, Markiewicz KH (2014) Surface-initiated RAFT/MADIX polymerization on xanthate-coated iron oxide nanoparticles. Macromol Chem Phys 215:190–197. https://doi.org/10.1002/macp.201300400
44. Misztalewska I, Wilczewska AZ, Wojtasik O, Markiewicz KH, Kuchlewski P, Majcher AM (2015) New acetylacetone-polymer modified nanoparticles as magnetically separable complexing agents. RSC Adv 5:100281–100289. https://doi.org/10.1039/C5RA20137C

45. Markiewicz KH, Niemirowicz-Laskowska K, Szymczuk D, Makarewicz K, Misztalewska-Turkowicz I, Wielgat P, Majcher-Fitas AM, Milewska S, Car H, Wilczewska AZ (2021) Magnetic particles with polymeric shells bearing cholesterol moieties sensitize breast cancer cells to low doses of doxorubicin. Int J Mol Sci 22:4898. https://doi.org/10.3390/ijms22094898
46. Ferlin F, Anastasiou I, Salameh N, Miyakoshi T, Baudoin O, Vaccaro L (2022) C(sp^3)−H arylation promoted by a heterogeneous palladium-N-heterocyclic carbene complex in batch and continuous flow. Chemsuschem 15:e202102736. https://doi.org/10.1002/cssc.202102736
47. Vijayakrishna K, Manojkumar K, Haribabu P, GyanaRanjan B, Tilottama B, Agirre A, Meabe L, Mantione D, Porcarelli L, Leiza R, J, Mecerreyes D, (2020) Morpholine-based RAFT agents for the reversible deactivation radical polymerization of vinyl acetate and *N*-vinylimidazole. Polym Int 69:883–890. https://doi.org/10.1002/pi.6032
48. Green MD, Allen MH, Dennis JM, la Cruz DS, Gao R, Winey KI, Long TE (2011) Tailoring macromolecular architecture with imidazole functionality: a perspective for controlled polymerization processes. Eur Polym J 47:486–496. https://doi.org/10.1016/j.eurpolymj.2010.09.035
49. Tilottama B, Manojkumar K, Haribabu PM, Vijayakrishna K (2022) A short review on RAFT polymerization of less activated monomers. J Macromol Sci Part A 59:180–201. https://doi.org/10.1080/10601325.2021.2024076
50. Balinge KR, Bhagat PR (2017) Palladium–N-heterocyclic carbene complexes for the Mizoroki-Heck reaction: an appraisal. Comptes Rendus Chim 20:773–804. https://doi.org/10.1016/j.crci.2017.03.003
51. Dolomanov OV, Bourhis LJ, Gildea RJ, Howard JAK, Puschmann H (2009) *OLEX2*: a complete structure solution, refinement and analysis program. J Appl Crystallogr 42:339–341. https://doi.org/10.1107/S0021889808042726
52. Sheldrick GM (2008) A short history of *SHELX*. Acta Crystallogr A 64:112–122. https://doi.org/10.1107/S0108767307043930
53. Sheldrick GM (2015) Crystal structure refinement with *SHELXL*. Acta Crystallogr Sect C Struct Chem 71:3–8. https://doi.org/10.1107/S2053229614024218